Supporting Information

Diagonally π-Extended Perylene-based Bis(heteroacene) for Chiroptical Activity and Integrating Luminescence with Carrier-transporting Capability

Bo Li,[†] *Wangwang Peng,*[†] *Shenglian Luo,*[‡] *Chuanling Jiang,*[⊥] *Jing Guo,*[§] *Sheng Xie,*[*†] *Yuanyuan Hu,*[*§] *Yang Zhang,*[†] *and Zebing Zeng*[*†]

[†] State Key Laboratory of Chemo/Biosensing and Chemometrics, College of Chemistry and Chemical Engineering, Hunan University, Changsha 410082, P. R. China.

[‡] College of Environmental and Chemical Engineering, Nanchang Hangkong University, Nanchang 330063, P. R. China.

[⊥] Department of Pharmacy, Clinic Medical College of Anhui Medical University, Hefei 230012, P. R. China.

[§] Key Laboratory for Micro-Nano Optoelectronic Devices of Ministry of Education, School of Physics and Electronics, Hunan University, Changsha 410082 , P. R. China..

Table of Contents

1. General method

Solvents were purified and dried by standard methods prior to use. All commercially available reagents were used without further purification unless otherwise noted. Column chromatography was generally performed on silica gel (200 - 300 mesh) and reactions were monitored by thin layer chromatography (TLC) using silica gel GF254 plates with UV light to visualize the course of reaction. ^{1}H and ^{13}C NMR data were recorded on a 400 MHz spectrometer at room temperature. All chemical shifts are quoted in ppm, relative to tetramethylsilane, using residual solvent peak as a reference standard. The following abbreviations were used to explain the multiplicities: s = singlet, d = doublet, m = multiplet. Cyclic voltammetry (CV) and differential pulse voltammetry (DPV) were performed on a Chenhua 650D electrochemical using a three-electrode cell with a glassy carbon working electrode, a platinum wire counter electrode, and a $Ag/AgNO_3$ or Ag/AgCl reference electrode in anhydrous solvents containing recrystallized tetra-*n*-butyl- ammoniumhexafluorophosphate ($TBAPF_6$, 0.1 M) as supporting electrolyte at 298 K. The potential was externally calibrated against the ferrocene/ferrocenium couple. Absorption spectra were recorded on a Shimadzu UV-3600 plus. Photoluminescence spectra were recorded on a Thermo Scientific Lumina. HR MALDI-TOF mass spectra recorded on Finnigan MAT TSQ 7000 instrument. Circular dichroism (CD) spectra were recorded on JASCO J-810 circular dichroismspectrometer.

2. Synthetic procedures

Synthesis of 2

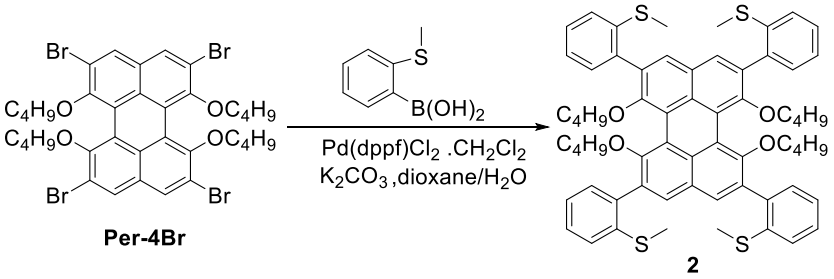

To a solution of compound **Per-4Br** [S1] (750.0 mg, 0.88 mmol) in dioxane (40 mL), 2-methylthiophenylboronic acid (706.3 mg, 4.20 mmol), Pd(dppf)Cl_2 CH_2Cl_2 (71.9 mg, 0.09 mmol) and aqueous solution K_2CO_3 (2.0 M, 5 mL) were added under argon atmosphere. The reaction mixture was stirred at 80 °C. The reaction was monitored by TLC to confirm consumption of starting material. Upon completion, the solution was diluted with dichloromethane (25 mL) and water (15 mL), and washed with brine (20 mL). After removal of the solvent, the residue was purified by silica gel chromatography (petroleum ether/dichloromethane = 3/1) to afford compound **2** (810 mg, 90%) as a yellow solid. ^{1}H NMR (400 MHz, $CDCl_3$) δ 7.61 - 7.60 (m, 4H), 7.35 - 7.21 (m, 16H), 4.02 - 3.68 (m, 4H), 3.17 - 3.07 (m, 4H), 2.40 - 2.35 (m, 12H), 1.28 - 1.25 (m, 8H), 0.94 - 0.87 (m, 8H), 0.63 (s, 12H). ^{13}C NMR (100 MHz, $CDCl_3$) δ 192.57, 154.30, 138.29, 133.34, 130.74, 128.63, 127.75, 123.84, 118.17, 32.37, 32.20, 18.86, 15.94, 15.54, 13.88. HRMS (MALDI-TOF, *m/z*) calcd for $C_{64}H_{68}O_4S_4$ $[M]^+$, 1028.4000; found 1028.3998 (error = - 0.19 ppm). m.p. = 168 ~ 180 °C.

Synthesis of 1

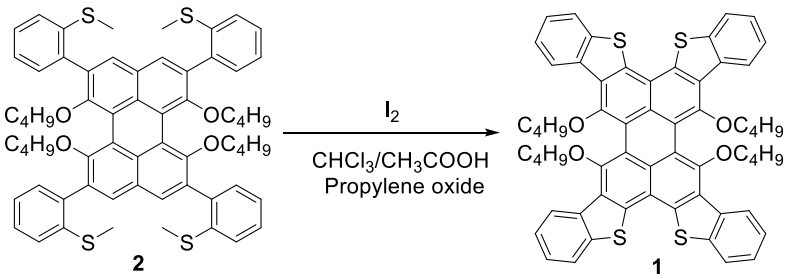

To a solution of compound **2** (6.0 g, 5.8 mmol) in chloroform (200 mL), acetic acid (150 mL), propylene oxide (200 mL) was added via a syringe. The solution was cooled to 0 ℃, and then iodine solution in chloroform (58.3 mmol) was slowly added. The mixture was heated to 55 ℃ and stirring for 12 h under inert atmosphere. The reaction was monitored by TLC to confirm consumption of starting material. Upon completion, the mixture was quenched with aqueous sodium bicarbonate, extracted with CH_2Cl_2 (15 mL) and dried by anhydrous $MgSO_4$. After removal of the solvent, the residue was purified by silica gel chromatography (petroleum ether/dichloromethane = 5/1) to afford compound **1** (5.0 g, 89%) as a yellow solid. ^{1}H NMR (400 MHz, toluene-d_8): δ 9.34 (d, J = 8.2 Hz, 4H), 7.83 (d, J = 8.0 Hz, 4H), 7.53 - 7.49 (m, 4H), 7.32 - 7.28 (m, 4H), 3.83 - 3.81 (m, 4H), 3.44 - 3.40 (m, 4H), 1.55 - 1.39 (m, 8H), 1.11 - 1.07 (m, 8H), 0.44 (t, J = 7.4Hz, 12H). ^{13}C NMR (100 MHz, $CDCl_3$): δ 154.91, 139.24, 135.63, 135.59, 134.01, 127.36, 126.22, 125.59, 124.93, 122.27, 116.27, 115.37, 32.51, 19.20, 13.54. HRMS (MALDI-TOF, *m/z*) calcd for $C_{60}H_{52}O_4S_4$ $[M]^+$, 964.2748; found: 964.2724 (error = -2.5 ppm). m.p. = 280 ~ 295 ℃.

3. Optimization of cyclization reaction

Table S1. Screening of reaction conditions.

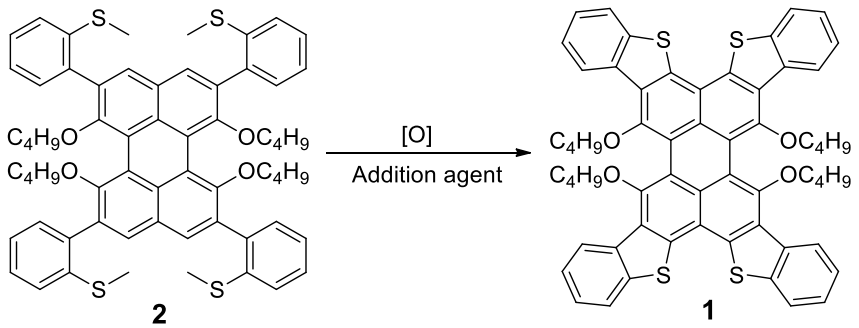

Entry	Conditions	Temperature	Product yield[c]
1[S2]	[a]I_2, $CHCl_3$	70 ℃~100 ℃	Trace
2	H_2O_2, HAc/DCM	RT	0
3[S3]	H_2O_2, HAc/DCM or H_2O_2,CF_3COOH/DCM	RT	0

4	H_2O_2, HAc/DCM or H_2O_2,CF_3COOH/Pydrine	RT	0
5	[a]I_2/$CHCl_3$, HAc	RT	1~3%
6	[a]I_2/$CHCl_3$, HAc/PO[b] (v/v = 2/1)	RT	29%
7	[a]I_2/$CHCl_3$, HAc/PO[b] (v/v = 1/1)	RT	52%
8	[a]I_2/$CHCl_3$, HAc/PO[b] (v/v = 3/4)	RT	75%
9	[a]I_2/$CHCl_3$, HAc/PO[b] (v/v = 1/2)	RT	70%
10	[a]I_2/$CHCl_3$, HAc/PO[b] (v/v = 3/4)	55 ℃	89%
11	[a]I_2/$CHCl_3$, HAc/PO[b] (v/v = 3/4)	70 ℃	84%

[a]10 equivalent relative to that of **2** in the reaction; [b]PO is propyleneoxide; [c]Isolated yield. All the testing reactions were carried out with 0.1 mmol of **2**.

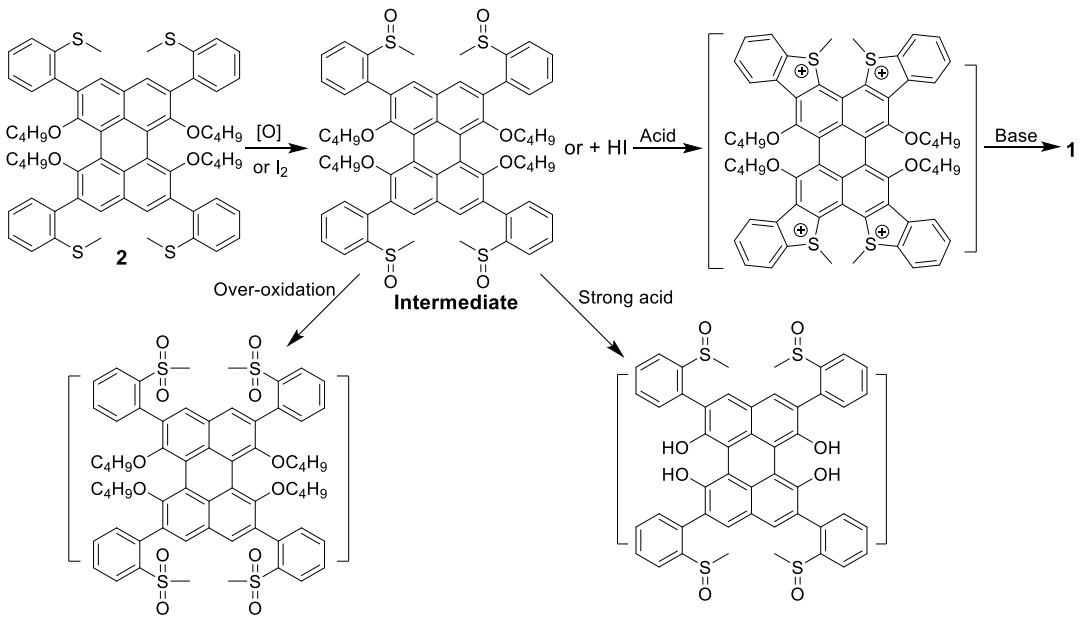

Scheme S1. Reaction mechanism was proposed for four-fold thienannulation on basis of acid-induced cyclization of aromatic methyl sulfoxide developed by K. Müllen[S4]. It is noteworthy that the previous synthetic methodology applied to substrate **2** gave either undesired products under strong oxidative condition or removal of alkoxyl groups (-OC_4H_9) in the strong acid, especially for generated HI when weaker oxidant I_2 was used in the reaction.

4. Detailed optical resolution of 1 by the chiral HPLC

Separation of the chiral isomers was performed on a Shimadzu LC-20AR instrument equipped with a Daicel Chiralcel OD-H column (4.6 mm × 250 mm). A

mixture of hexane/isopropanol (99 : 1) was used as the eluent at a flow rate of 1 mL/min.

5. Investigation of conformational stability by CD spectroscopy

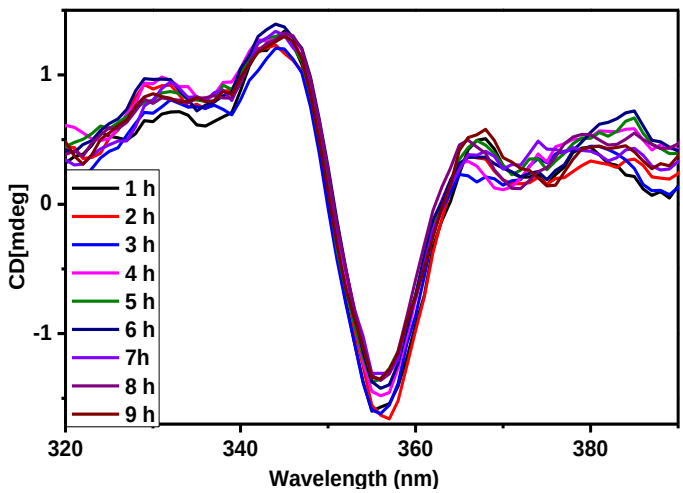

Figure S1. Thermal racemization of the second-eluted enantiomer *(M, M)*-**1** in toulene at 70 ℃ was monitored by CD spectrum following the decay of the enantiomeric excess over time.

The spectral changes (Figure S1) were monitored at 344 and 356 nm. Plotting the average ln ($\Delta\varepsilon/\Delta\varepsilon_0$)-values vs time resulted in $k = 6.6\times10^{-12} \pm 0.1\times10^{-12}$ after linear regression. According to

$$\Delta G = -RT\ln K^{\#} \quad \text{(Van't Hoff equation)}$$

$$K^{\#} = \frac{k\times h}{\kappa\times k_b\times T} \quad \text{(Eyring equation)}^{[S5]}$$

(h: Plancks constant, k_b: Boltzmann constant)

$\Delta G^{\#}$ was calculated to be 34.6 ± 0.4 kcal/mol

For the enantiomer interconversion of **1**, where a stepwise process converts one enantiomer into the unstable meso form and then into the other enantiomer (see the theoretical section below), the statistical transmission coefficient $\kappa = 0.5$ was used in the calculation of the free energy barrier $\Delta G^{\#}$ for a single inversion (*M, M* or *P, P* to meso) from the rate constant of the overall process.

6. Dynamic investigation of 1 by VT proton NMR spectra

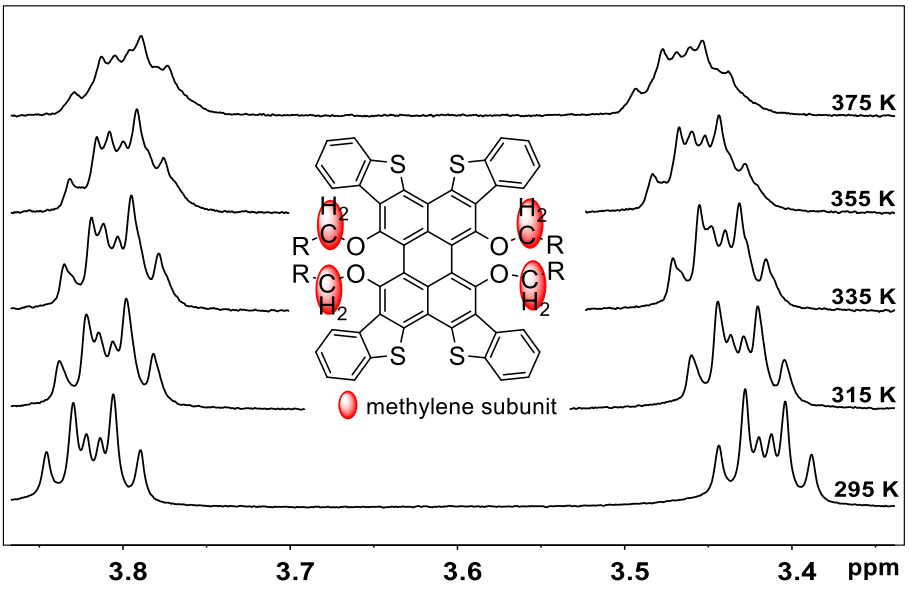

Figure S2. Temperature-dependent ^{1}H NMR spectra of racemic **1** in toluene-d_8, the signals represent proton resonances of methylene subunits (-OCH_2-).

7. Cyclic voltammograms of 1

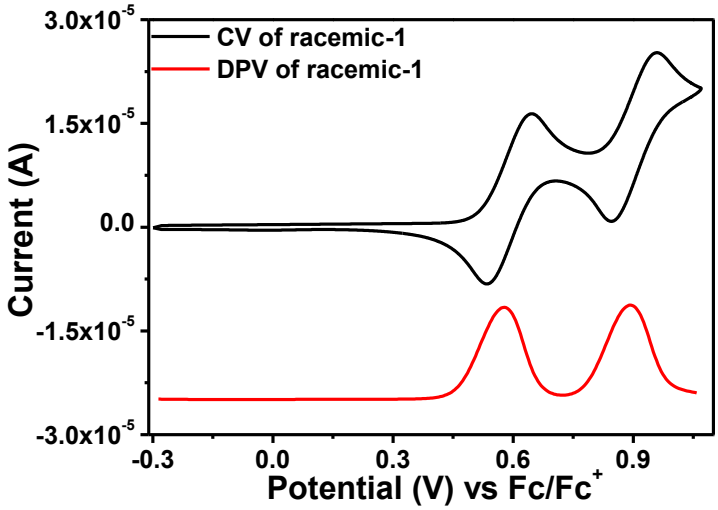

Figure S3. Cyclic voltammograms (black curves) and differential pulse voltammograms (red curves) of 1 solution in DCM (1.0 mM), redox potentials were determined by using 0.10 M n-$Bu_4N^+PF_6^-$ as a supporting electrolyte, the electrode potential was externally calibrated by the ferrocene/ferrocenium redox couple. (Eox^1 = 0.52 V, Eox^2 = 0.84 V, E_{HOMO} = -5.32 eV).

8. X-ray crystallographic 1

The single crystal was grown by slowly diffusing petroleum ether vapor into the dichloromethane solution of compound **1**.

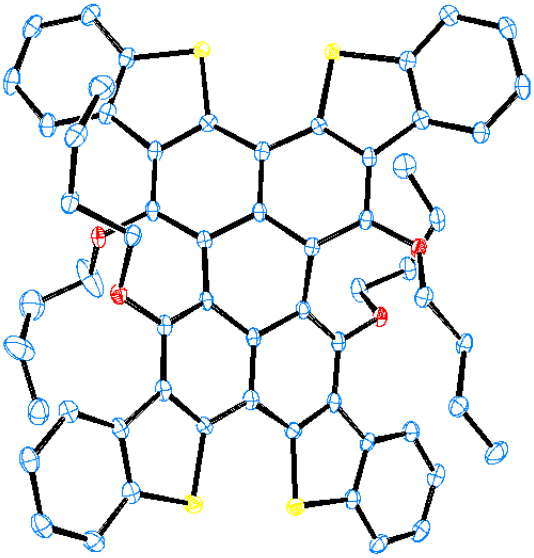

Figure S4. ORTEP plots of crystal **1** (carbon, blue; oxygen, red; sulphur, yellow; hydrogen atoms are omitted for clarity, and thermal ellipsoids are shown at 50%)

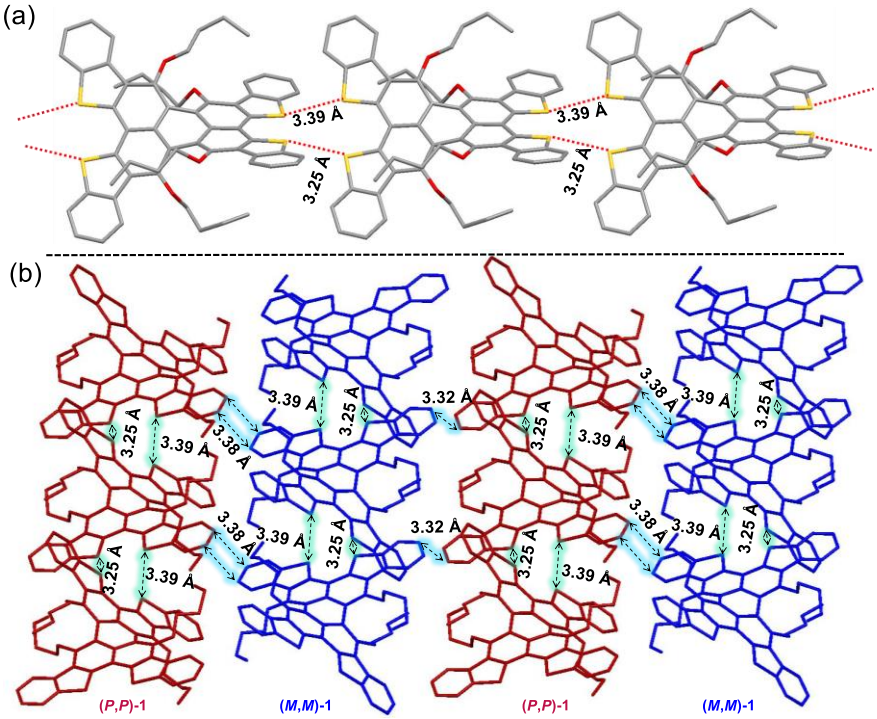

Figure S5. The rich and close S ··S contacts (3.39 ~ 3.32 Å) were observed for nearing enantiomers (a), and molecular packing arrangements of racemic 1 (b). Hydrogen atoms are omitted for clarity.

9. 1-based OFETs and AFM measurements

9.1 Thin film deposition and device fabrication

Bottom-gate/bottom-contact OFET devices fabricated using Si/SiO_2 substrates where Si and SiO_2 work as gate electrode and gate dielectric, respectively. The source and drain gold electrodes with thickness of 50 nm using 2 nm of chromium as an adhesion layer were formed by standard lithography procedures. Prior to deposition, the wafers were cleaned up with ultrapure water, acetone, isopropanol, and then treated by oxygen plasma and passivated by trichloro(octadecyl)silane to reduce the traps. Finally, then films were deposited (5 mg/mL in THF) by spin-coating at 1500 rpm in a nitrogen glovebox. The length and width of channel were 80 μm and 1000 μm, respectively.

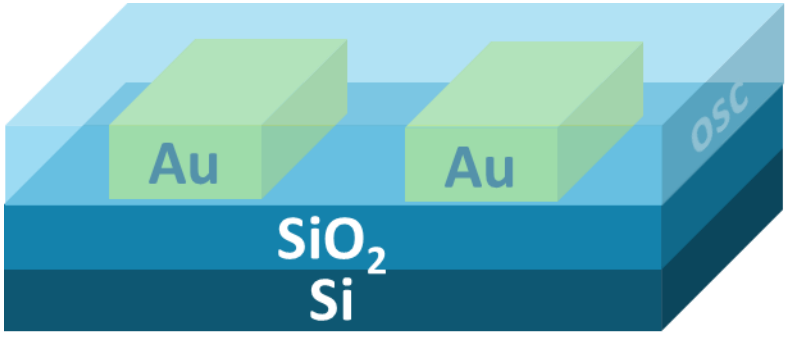

Figure S6. The organic field-effect transistors (OFETs) devices were successfully fabricated in a bottom-contact bottom-gate (BGBC) configuration.

9.2 The parameters of charge carrier mobilities

The charge carrier mobilities of OFETs were calculated in the saturation regime from a plot of the square root of the drain current vs. gate voltage using the following equation:

$$I_{DS} = \frac{WC_i}{2L}\mu(V_G - V_T)^2$$

where I_{DS} is the drain-source current, C_i is the capacitance per unit area of the gate dielectric(10 nF/cm^2), L is the channel length, W is the channel width, V_G and V_T are the gate-source voltage and threshold voltage, respectively .

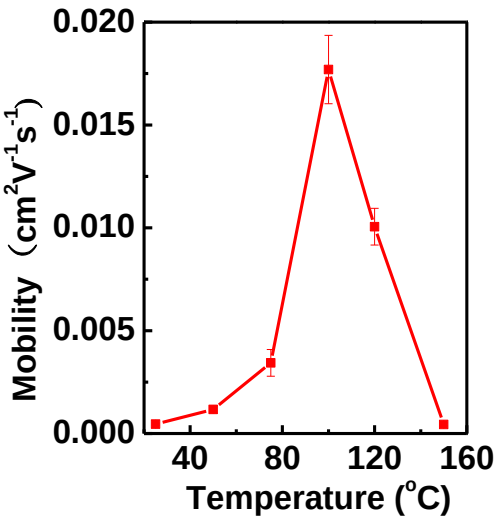

Figure S7. Temperature-dependent characteristics and the average carrier mobility (0.017 cm^2 V^{-1}s^{-1}) in devices.

Table S2. Electronic performances based on thin films of **1**

Compound	μ_h cm^{2}V^{-1}s^{-1}	I_{on}/I_{off}	V_T/V	channel width(μm)	channel length(μm)
1	0.02	2.3×10^3	31.3	80	1000

9.3 Topographical images of **1** at different substrate temperature (t_{sub}).

AFM measurements were performed using XE7 (Park SYSTEMS), operated in intermittent contact (tapping) mode, at a scanning speed of 1 Hz.

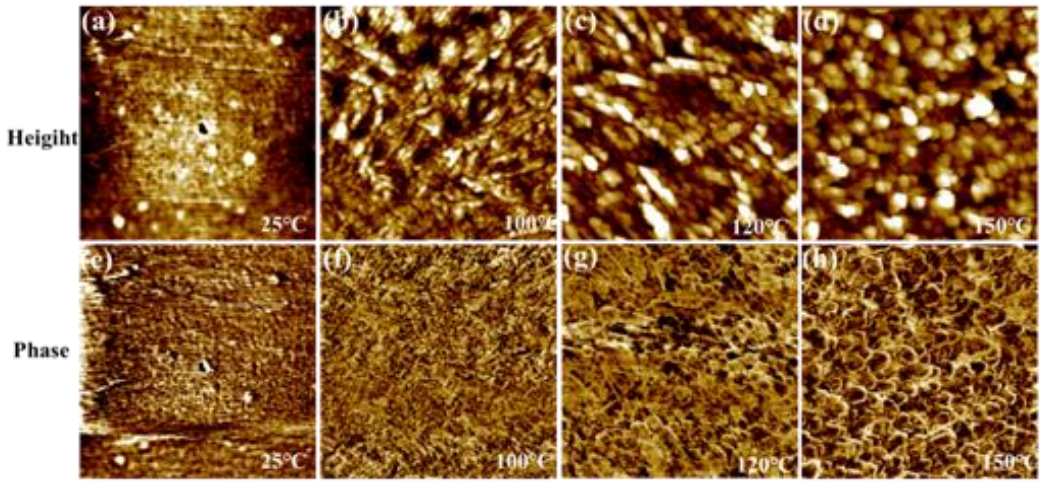

Figure S8. (a-d) AFM height and (e-h) phase images of thin film **1** on OTS-treated SiO_2 substrates annealed at 25 ℃, 100 ℃, 120 ℃, 150 ℃.

10. DFT and TD-DFT calculations

Density functional theory (DFT) and time-dependent DFT (TD-DFT) simulations were performed using the Gaussian 09 software package.[S6] All calculations were carried out using the DFT method with Becke's three-parameter hybrid exchange functionals and the Lee-Yang-Parr correlation functional (B3LYP) employing the 6-31G (d,p) basis set for all atoms.[S7]

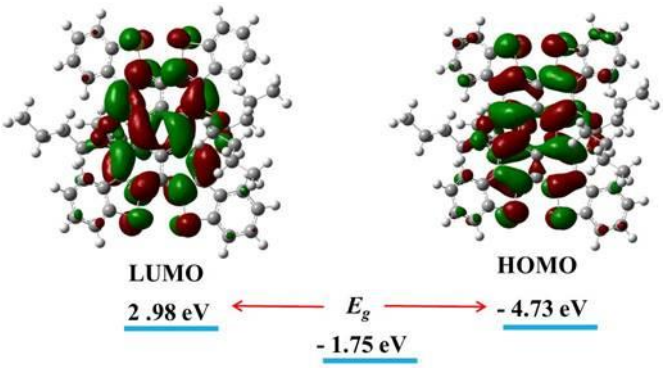

Figure S9. LUMOs (left) and HOMOs (right) of **1** obtained from DFT calculations at the B3LYP/6-31G (d,p) level.

TD-DFT

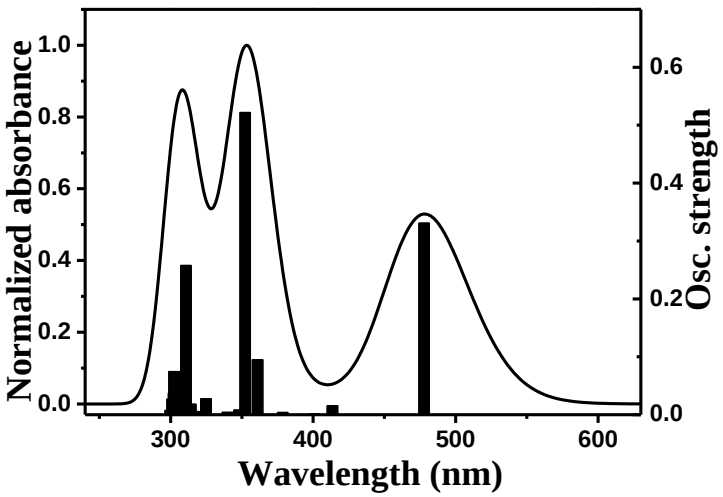

Figure S10. Calculated (B3LYP/6-31G (d,p)) absorption spectra and oscillator strengths of **1**.

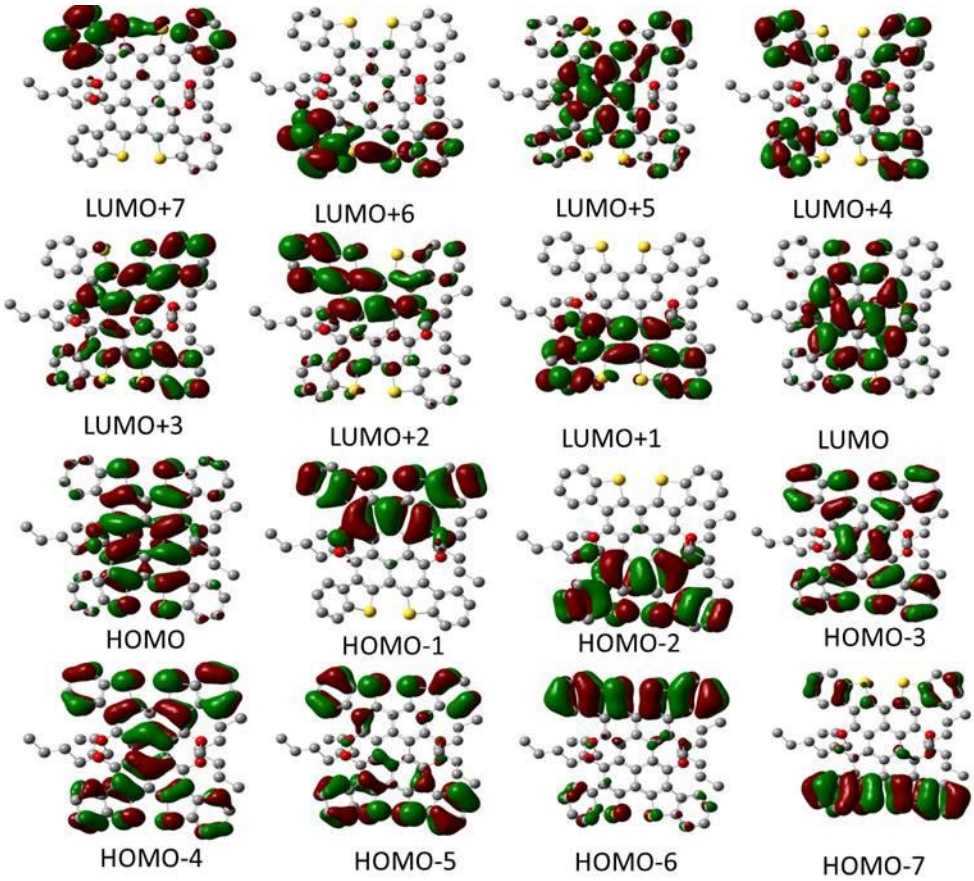

Figure S11. LUMOs and HOMOs of molecule **1**, obtained by DFT calculations at the B3LYP/6-31G(d,p) level

Major electronic transitions of **1** calculated by TD-DFT method.

excited state	Energy (eV)	Wavelength (nm)	Osc. Strength	Major contribs
1	20924.44155	477.91001	0.3308	HOMO→LUMO (99%)
2	24180.50178	413.55635	0.0158	HOMO-2→LUMO (17%), HOMO→LUMO+1 (80%)
3	24941.08261	400.94491	0.0016	HOMO-1→LUMO (36%), HOMO→LUMO+2 (50%)
4	26409.81822	378.64706	0.0042	HOMO→LUMO +2 (24%), HOMO→LUMO +3 (69%)
5	27701.11186	360.99634	0.0952	HOMO-2→LUMO (44%), HOMO-1→LUMO (29%)
6	28381.8438	352.33793	0.5221	HOMO-2→LUMO (31%), HOMO-1→LUMO (29%), HOMO→LUMO+2 (14%), HOMO→LUMO+3 (12%)
7	28731.88842	348.04534	0.0082	HOMO -3→LUMO (86%)
8	29421.49246	339.88758	0.0044	HOMO-4→LUMO (93%)
9	30789.40877	324.78701	0.0275	HOMO→LUMO+4 (19%), HOMO→LUMO+5 (63%)
10	31605.64185	316.39921	0.0057	HOMO-2→LUMO+1(10%), HOMO-1→LUMO+1(30%), HOMO→LUMO+4 (39%), HOMO→LUMO +5 (12%)
11	31838.73608	314.08282	0.0183	HOMO-1→LUMO+1(63%), HOMO→LUMO +4 (26%)
12	32183.94138	310.71396	0.2577	HOMO-6→LUMO (11%), HOMO-2→LUMO+1(45%), HOMO-1→LUMO+2 (13%)
13	32408.16351	308.56423	0.0184	HOMO -5→LUMO (86%)
14	32589.63826	306.846	0.0012	HOMO→LUMO +6 (45%),

15	32792.88997	304.94415	0.0745	HOMO→LUMO +8 (32%) HOMO-1→LUMO+2(26%), HOMO-1→LUMO+3 (25%)

11. Detailed crystallographic data

Table S3. Crystal data and structure refinement for **1** (CCDC:1882923)

Identification code	1
Empirical formula	$C_{60}H_{52}O_4S_4$
Formula weight	965.25
Temperature/K	100.00(10)
Crystal system	triclinic
Space group	P-1
a/Å	13.2096(4)
b/Å	13.4878(3)
c/Å	15.1291(3)
α/°	85.310(2)
β/°	79.985(2)
γ/°	60.706(3)
Volume/$Å^3$	2314.99(12)
Z	2
ρ_{calc}g/cm^3	1.385
μ/mm^{-1}	2.292
F(000)	1016.0
Crystal size/mm^3	0.2 × 0.18 × 0.15
Radiation	CuKα (λ = 1.54184)
2Θ range for data collection/°	7.516 to 143.782
Index ranges	-16 ≤ h ≤ 16, -16 ≤ k ≤ 16, -18 ≤ l ≤ 18
Reflections collected	32665
Independent reflections	8979 [R_{int} = 0.0554, R_{sigma} = 0.0517]
Data/restraints/parameters	8979/0/617
Goodness-of-fit on F^2	1.037
Final R indexes [I>=2σ (I)]	R_1 = 0.0699, wR_2 = 0.1886
Final R indexes [all data]	R_1 = 0.0818, wR_2 = 0.1964
Largest diff. peak/hole / e $Å^{-3}$	2.50/-0.68

Table S4. Bond Lengths [Å] for **1**.

Atom	Atom	Length/Å	Atom	Atom	Length/Å
S4	C15	1.743(3)			

S4	C14	1.748(3)
S1	C36	1.742(3)
S1	C37	1.750(3)
S3	C17	1.741(3)
S3	C18	1.741(3)
S2	C34	1.743(3)
S2	C33	1.739(3)
O2	C26	1.361(3)
O2	C53	1.445(4)
O3	C25	1.376(4)
O3	C57	1.448(5)
O4	C7	1.364(3)
O4	C49	1.450(3)
O1	C44	1.372(3)
O1	C45	1.445(3)
C6	C1	1.473(4)
C6	C5	1.438(4)
C6	C7	1.385(4)
C15	C16	1.427(4)
C15	C8	1.392(4)
C35	C2	1.409(4)
C35	C34	1.422(4)
C35	C36	1.426(4)
C42	C41	1.412(4)
C42	C37	1.399(4)
C42	C43	1.460(4)
C16	C5	1.414(4)
C16	C17	1.422(4)
C3	C2	1.438(4)
C3	C4	1.480(4)
C3	C26	1.395(4)
C2	C1	1.430(4)
C34	C27	1.395(4)
C1	C44	1.388(4)
C5-	C4	1.435(4)
C28	C29	1.405(4)
C28	C27	1.462(4)
C28	C33	1.408(4)
C36	C43	1.392(4)
C24	C17	1.393(4)
C24	C23	1.459(4)
C24	C25	1.412(4)
C8	C7	1.419(4)
C8	C9	1.454(4)
C4	C25	1.395(4)
C29	C30	1.388(4)
C13	C12	1.385(4)
C13	C14	1.395(4)
C9	C10	1.412(4)
C9	C14	1.405(4)
C10	C11	1.379(5)
C23	C18	1.404(5)
C23	C22	1.407(4)
C30	C31	1.400(5)
C32	C31	1.378(5)
C32	C33	1.397(4)
C41	C40	1.383(4)
C27	C26	1.423(4)
C49	C50	1.519(4)
C12	C11	1.396(5)
C37	C38	1.394(4)
C40	C39	1.399(5)
C19	C18	1.395(4)
C19	C20	1.381(5)
C53	C54	1.511(4)
C43	C44	1.412(4)
C54	C55	1.527(5)
C38	C39	1.382(5)
C47	C46	1.523(5)
C47	C48	1.530(5)
C51	C50	1.522(4)
C51	C52	1.525(5)
C22	C21	1.390(5)
C20	C21	1.390(5)
C46	C45	1.517(4)
C55	C56	1.525(5)
C60	C59	1.521(6)
C57	C58	1.485(6)
C59	C58	1.472(6)

Table S5. Bond Angles [°] for **1**.

Atom	Atom	Atom	Angle/°
C15	S4	C14	91.36(14)
C36	S1	C37	91.26(14)
C17	S3	C18	91.29(15)
C33	S2	C34	91.12(14)
C26	O2	C53	120.3(2)
C25	O3	C57	113.6(2)
C7	O4	C49	119.3(2)
C44	O1	C45	114.8(2)
C5	C6	C1	115.5(3)
C7	C6	C1	125.6(3)
C7	C6	C5	118.9(3)
C16	C15	S4	125.0(2)
C8	C15	S4	112.5(2)
C8	C15	C16	122.2(3)
C2	C35	C34	116.8(3)
C2	C35	C36	117.1(3)
C34	C35	C36	126.1(3)
C41	C42	C43	130.0(3)
C37	C42	C41	118.0(3)
C37	C42	C43	111.9(3)
C5	C16	C15	116.1(3)
C5	C16	C17	116.9(3)
C17	C16	C15	127.0(3)
C2	C3	C4	115.7(2)
C26	C3	C2	118.2(3)
C26	C3	C4	125.9(3)
C35	C2	C3	121.4(3)
C35	C2	C1	120.1(3)
C1	C2	C3	118.5(3)
C35	C34	S2	124.9(2)
C27	C34	S2	113.1(2)
C27	C34	C35	121.9(3)
C2	C1	C6	117.2(3)
C44	C1	C6	123.3(3)
C44	C1	C2	119.6(3)
C16	C5	C6	120.6(3)
C16	C5	C4	120.9(3)
C4	C5	C6	118.5(3)
C29	C28	C27	130.7(3)
C29	C28	C33	118.1(3)
C33	C28	C27	111.2(3)
C35	C36	S1	125.0(2)
C43	C36	S1	112.9(2)
C43	C36	C35	122.0(3)
C17	C24	C23	111.8(3)
C17	C24	C25	119.5(3)
C25	C24	C23	128.7(3)
C15	C8	C7	119.5(3)
C15	C8	C9	112.2(3)
C7	C8	C9	128.3(3)
C5	C4	C3	117.0(3)
C25	C4	C3	124.5(3)
C25	C4	C5	118.5(3)
C16	C17	S3	125.0(2)
C24	C17	S3	112.9(2)
C24	C17	C16	122.1(3)
C30	C29	C28	119.0(3)
O4	C7	C6	124.8(3)
O4	C7	C8	115.8(3)
C6	C7	C8	119.4(3)
C12	C13	C14	117.7(3)
C10	C9	C8	130.2(3)
C14	C9	C8	111.6(3)
C14	C9	C10	118.1(3)
C11	C10	C9	119.2(3)
C18	C23	C24	111.4(3)
C18	C23	C22	118.2(3)
C22	C23	C24	130.3(3)
C29	C30	C31	121.7(3)
C31	C32	C33	118.1(3)
C40	C41	C42	119.1(3)
C34	C27	C28	111.7(3)
C34	C27	C26	119.7(3)
C26	C27	C28	128.6(3)
O3	C25	C24	118.1(2)

O3	C25	C4	121.4(3)	C53	C54	C55	113.4(3)
C4	C25	C24	120.4(3)	C39	C38	C37	117.9(3)
O4	C49	C50	109.0(2)	O1	C44	C1	121.5(3)
C13	C12	C11	120.6(3)	O1	C44	C43	118.6(3)
O2	C26	C3	125.6(3)	C1	C44	C43	119.8(3)
O2	C26	C27	114.5(2)	C46	C47	C48	113.2(3)
C3	C26	C27	119.9(3)	C28	C33	S2	112.9(2)
C42	C37	S1	112.2(2)	C32	C33	S2	124.4(3)
C38	C37	S1	124.8(3)	C32	C33	C28	122.7(3)
C38	C37	C42	123.0(3)	C38	C39	C40	120.4(3)
C13	C14	S4	125.0(2)	C10	C11	C12	121.6(3)
C13	C14	C9	122.7(3)	C50	C51	C52	112.3(3)
C9	C14	S4	112.2(2)	C49	C50	C51	112.8(3)
C41	C40	C39	121.6(3)	C21	C22	C23	119.0(3)
C20	C19	C18	118.1(3)	C19	C20	C21	120.6(3)
O2	C53	C54	107.1(2)	C45	C46	C47	115.2(3)
C23	C18	S3	112.6(2)	O1	C45	C46	107.8(2)
C19	C18	S3	124.8(3)	C22	C21	C20	121.6(3)
C19	C18	C23	122.5(3)	C56	C55	C54	113.4(3)
C32	C31	C30	120.3(3)	O3	C57	C58	111.0(3)
C36	C43	C42	111.6(3)	C58	C59	C60	118.4(4)
C36	C43	C44	119.4(3)	C59	C58	C57	118.0(4)
C44	C43	C42	128.8(3)				

Table S6. Torsion Angles [º] for **1**.

A	B	C	D	Angle/˚	A	B	C	D	Angle/˚
S4	C15	C16	C5	-177.0(2)	C4	C3	C26	C27	165.4(3)
S4	C15	C16	C17	0.3(4)	C17	S3	C18	C23	0.8(2)
S4	C15	C8	C7	-174.7(2)	C17	S3	C18	C19	-179.0(3)
S4	C15	C8	C9	4.4(3)	C17	C16	C5	C6	169.9(3)
S1	C36	C43	C42	0.0(3)	C17	C16	C5	C4	-10.9(4)
S1	C36	C43	C44	-177.3(2)	C17	C24	C23	C18	-0.5(4)
S1	C37	C38	C39	-179.3(2)	C17	C24	C23	C22	179.4(3)
S2	C34	C27	C28	1.7(3)	C17	C24	C25	O3	176.5(3)
S2	C34	C27	C26	-175.4(2)	C17	C24	C25	C4	-0.2(4)
O2	C53	C54	C55	-179.5(2)	C29	C28	C27	C34	179.4(3)
O3	C57	C58	C59	-70.3(6)	C29	C28	C27	C26	-3.8(5)
O4	C49	C50	C51	-162.1(2)	C29	C28	C33	S2	-179.8(2)
C6	C1	C44	O1	-7.5(4)	C29	C28	C33	C32	1.2(5)
C6	C1	C44	C43	168.4(3)	C29	C30	C31	C32	0.4(5)

C6	C5	C4	C3	15.0(4)	C7	O4	C49	C50	143.6(3)
C6	C5	C4	C25	-164.9(3)	C7	C6	C1	C2	141.2(3)
C15	S4	C14	C13	-175.7(3)	C7	C6	C1	C44	-38.9(4)
C15	S4	C14	C9	1.5(2)	C7	C6	C5	C16	21.4(4)
C15	C16	C5	C6	-12.5(4)	C7	C6	C5	C4	-157.8(3)
C15	C16	C5	C4	166.7(3)	C7	C8	C9	C10	-7.7(5)
C15	C16	C17	S3	4.9(4)	C7	C8	C9	C14	175.8(3)
C15	C16	C17	C24	-177.0(3)	C13	C12	C11	C10	0.6(4)
C15	C8	C7	O4	175.2(2)	C9	C8	C7	O4	-3.8(4)
C15	C8	C7	C6	-2.3(4)	C9	C8	C7	C6	178.7(3)
C15	C8	C9	C10	173.3(3)	C9	C10	C11	C12	-1.4(4)
C15	C8	C9	C14	-3.3(3)	C10	C9	C14	S4	-176.4(2)
C35	C2	C1	C6	-162.6(3)	C10	C9	C14	C13	0.9(4)
C35	C2	C1	C44	17.5(4)	C23	C24	C17	S3	1.1(3)
C35	C34	C27	C28	-175.3(3)	C23	C24	C17	C16	-177.2(3)
C35	C34	C27	C26	7.6(4)	C23	C24	C25	O3	-0.5(4)
C35	C36	C43	C42	-176.5(3)	C23	C24	C25	C4	-177.2(3)
C35	C36	C43	C44	6.1(4)	C23	C22	C21	C20	0.3(5)
C42	C41	C40	C39	0.5(5)	C41	C42	C37	S1	179.1(2)
C42	C37	C38	C39	-0.1(5)	C41	C42	C37	C38	-0.1(4)
C42	C43	C44	O1	-0.7(4)	C41	C42	C43	C36	-178.6(3)
C42	C43	C44	C1	-176.8(3)	C41	C42	C43	C44	-1.6(5)
C16	C15	C8	C7	11.3(4)	C41	C40	C39	C38	-0.9(5)
C16	C15	C8	C9	-169.5(3)	C27	C28	C29	C30	177.2(3)
C16	C5	C4	C3	-164.2(3)	C27	C28	C33	S2	1.3(3)
C16	C5	C4	C25	15.9(4)	C27	C28	C33	C32	-177.6(3)
C3	C2	C1	C6	16.5(4)	C25	O3	C57	C58	179.8(3)
C3	C2	C1	C44	-163.4(3)	C25	C24	C17	S3	-176.4(2)
C3	C4	C25	O3	-6.6(5)	C25	C24	C17	C16	5.3(4)
C3	C4	C25	C24	170.0(3)	C25	C24	C23	C18	176.7(3)
C2	C35	C34	S2	-178.7(2)	C25	C24	C23	C22	-3.4(5)
C2	C35	C34	C27	-2.1(4)	C49	O4	C7	C6	-46.2(4)
C2	C35	C36	S1	-176.6(2)	C49	O4	C7	C8	136.5(3)
C2	C35	C36	C43	-0.4(4)	C12	C13	C14	S4	175.3(2)
C2	C3	C4	C5	-37.4(4)	C12	C13	C14	C9	-1.7(4)
C2	C3	C4	C25	142.5(3)	C26	O2	C53	C54	163.5(2)
C2	C3	C26	O2	172.1(3)	C26	C3	C2	C35	17.2(4)
C2	C3	C26	C27	-11.4(4)	C26	C3	C2	C1	-161.9(3)
C2	C1	C44	O1	172.4(2)	C26	C3	C4	C5	145.8(3)
C2	C1	C44	C43	-11.7(4)	C26	C3	C4	C25	-34.3(5)

C34	S2	C33	C28	-0.4(2)	C37	S1	C36	C35	176.8(3)
C34	S2	C33	C32	178.6(3)	C37	S1	C36	C43	0.3(2)
C34	C35	C2	C3	-10.4(4)	C37	C42	C41	C40	0.0(4)
C34	C35	C2	C1	168.7(3)	C37	C42	C43	C36	-0.5(4)
C34	C35	C36	S1	3.5(4)	C37	C42	C43	C44	176.6(3)
C34	C35	C36	C43	179.6(3)	C37	C38	C39	C40	0.6(5)
C34	C27	C26	O2	176.4(3)	C14	S4	C15	C16	170.3(3)
C34	C27	C26	C3	-0.5(4)	C14	S4	C15	C8	-3.5(2)
C1	C6	C5	C16	-158.4(3)	C14	C13	C12	C11	0.9(4)
C1	C6	C5	C4	22.5(4)	C14	C9	C10	C11	0.6(4)
C1	C6	C7	O4	-11.0(5)	C19	C20	C21	C22	-1.0(5)
C1	C6	C7	C8	166.2(3)	C53	O2	C26	C3	-46.4(4)
C5	C6	C1	C2	-39.0(4)	C53	O2	C26	C27	136.9(3)
C5	C6	C1	C44	140.9(3)	C53	C54	C55	C56	75.9(4)
C5	C6	C7	O4	169.2(3)	C18	S3	C17	C16	177.1(3)
C5	C6	C7	C8	-13.5(4)	C18	S3	C17	C24	-1.1(2)
C5	C16	C17	S3	-177.8(2)	C18	C23	C22	C21	0.4(4)
C5	C16	C17	C24	0.3(4)	C18	C19	C20	C21	0.9(5)
C5	C4	C25	O3	173.3(3)	C31	C32	C33	S2	-179.1(2)
C5	C4	C25	C24	-10.1(4)	C31	C32	C33	C28	-0.2(5)
C28	C29	C30	C31	0.7(5)	C43	C42	C41	C40	178.0(3)
C28	C27	C26	O2	-0.2(4)	C43	C42	C37	S1	0.7(3)
C28	C27	C26	C3	-177.1(3)	C43	C42	C37	C38	-178.6(3)
C36	S1	C37	C42	-0.6(2)	C44	O1	C45	C46	-177.6(3)
C36	S1	C37	C38	178.7(3)	C47	C46	C45	O1	-70.2(4)
C36	C35	C2	C3	169.7(3)	C33	S2	C34	C35	176.1(3)
C36	C35	C2	C1	-11.2(4)	C33	S2	C34	C27	-0.8(2)
C36	C35	C34	S2	1.2(4)	C33	C28	C29	C30	-1.4(4)
C36	C35	C34	C27	177.9(3)	C33	C28	C27	C34	-1.9(4)
C36	C43	C44	O1	176.2(3)	C33	C28	C27	C26	174.9(3)
C36	C43	C44	C1	0.1(4)	C33	C32	C31	C30	-0.6(5)
C24	C23	C18	S3	-0.4(3)	C22	C23	C18	S3	179.7(2)
C24	C23	C18	C19	179.4(3)	C22	C23	C18	C19	-0.5(4)
C24	C23	C22	C21	-179.5(3)	C20	C19	C18	S3	179.6(2)
C8	C15	C16	C5	-3.8(4)	C20	C19	C18	C23	-0.2(5)
C8	C15	C16	C17	173.5(3)	C45	O1	C44	C1	-78.8(4)
C8	C9	C10	C11	-175.8(3)	C45	O1	C44	C43	105.2(3)
C8	C9	C14	S4	0.7(3)	C52	C51	C50	C49	176.7(3)
C8	C9	C14	C13	177.9(3)	C48	C47	C46	C45	-73.8(4)
C4	C3	C2	C35	-159.9(3)	C60	C59	C58	C57	-84.2(5)

C4	C3	C2	C1	21.0(4)	C57	O3	C25	C24	108.4(4)
C4	C3	C26	O2	-11.2(5)	C57	O3	C25	C4	-74.9(4)

12. NMR/mass spectra for new compounds

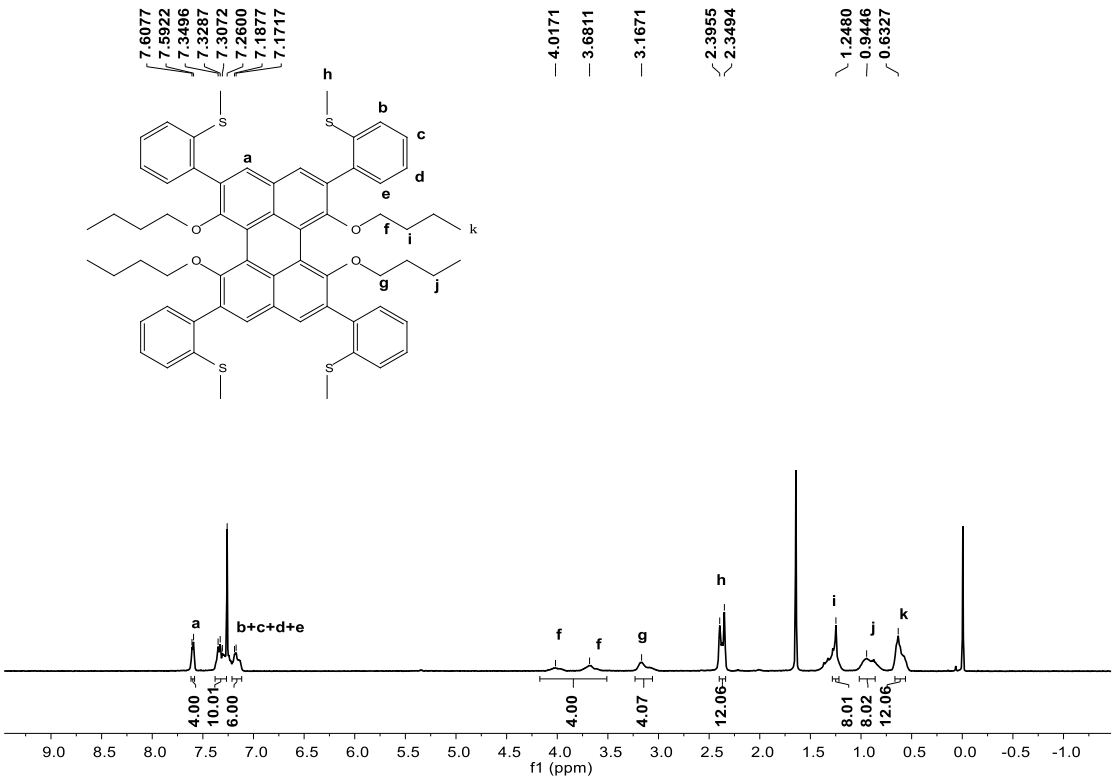

Figure S12. ^{1}H NMR spectrum (400 MHz) of compound **2** in $CDCl_3$ at 298 K.

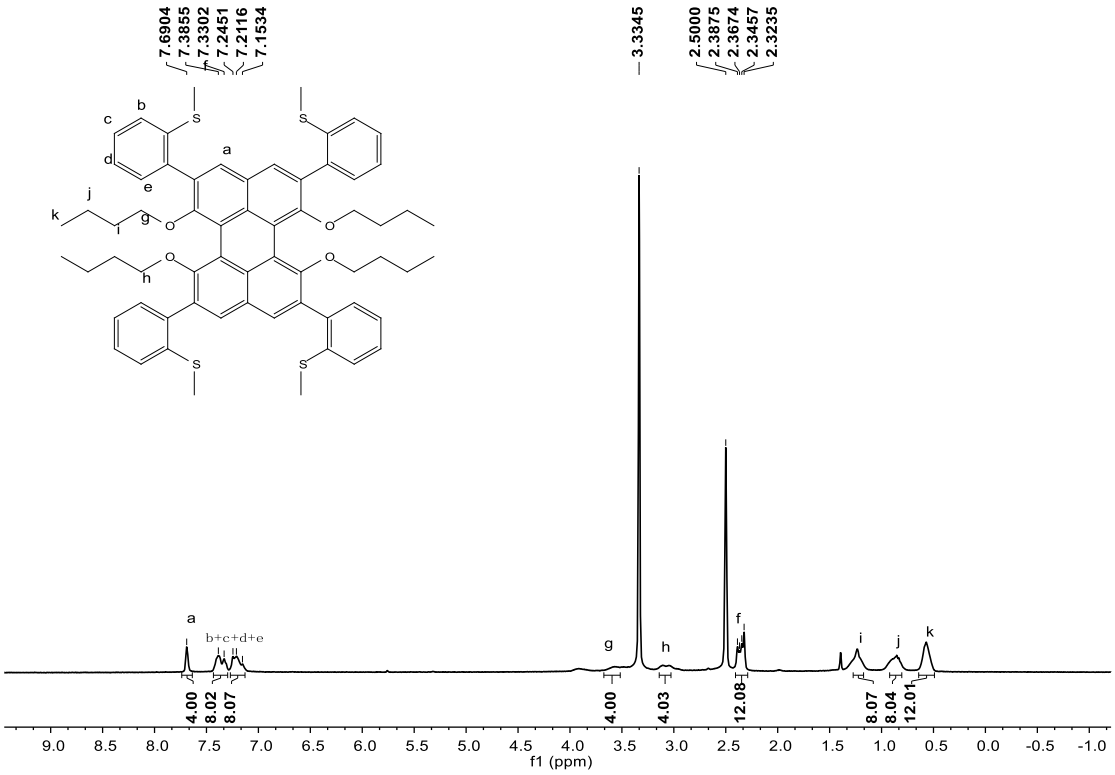

Figure S13. ^{1}H NMR spectrum (400 MHz) of compound **2** in DMSO-d_6 at 353 K.

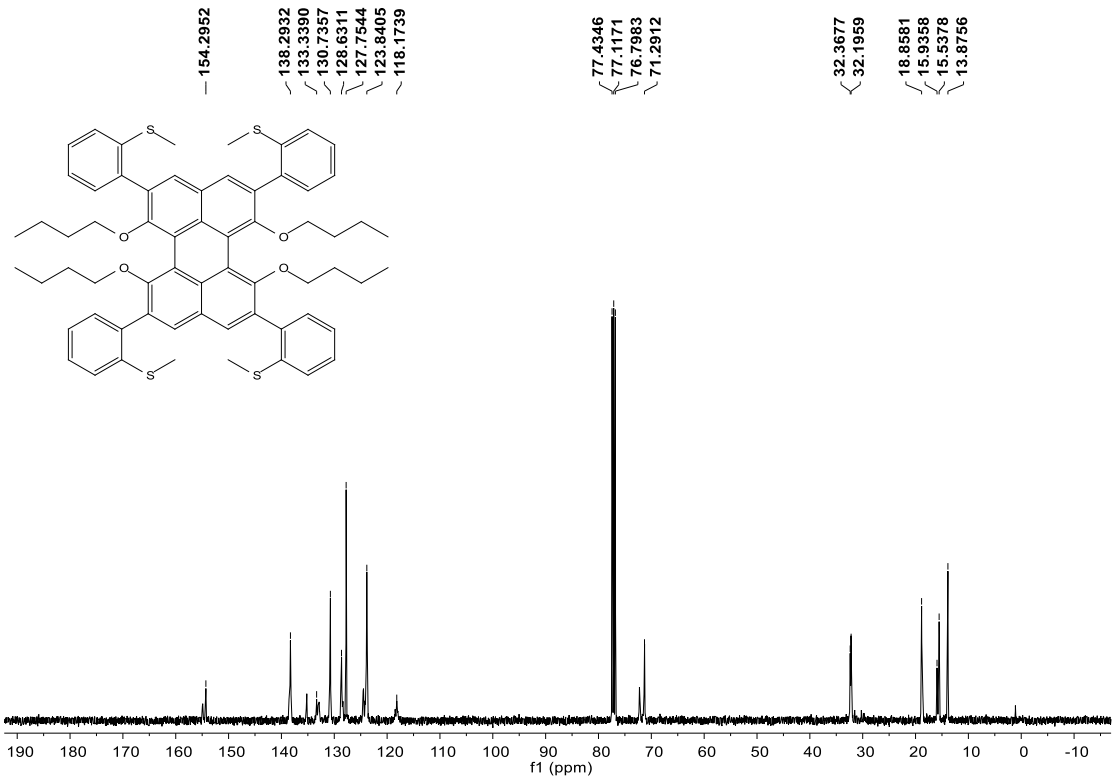

Figure S14. ^{13}C NMR spectrum (100 MHz) of compound **2** in $CDCl_3$ at 298 K.

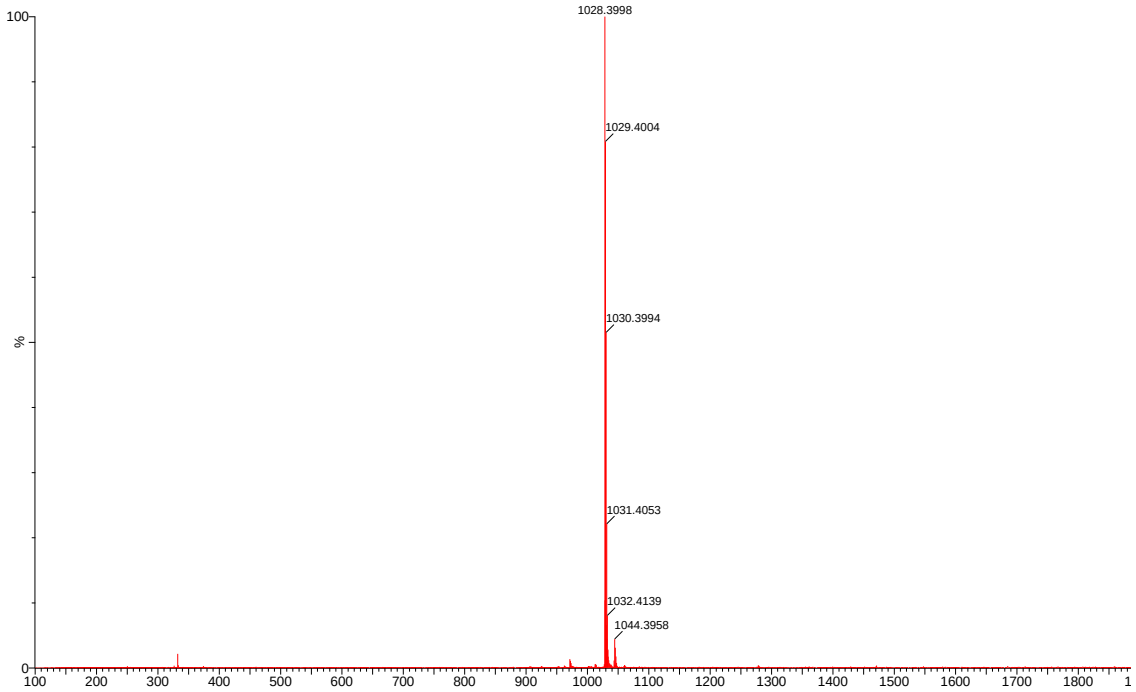

Figure S15. HR (MALDI-TOF) mass spectrum of **2**.

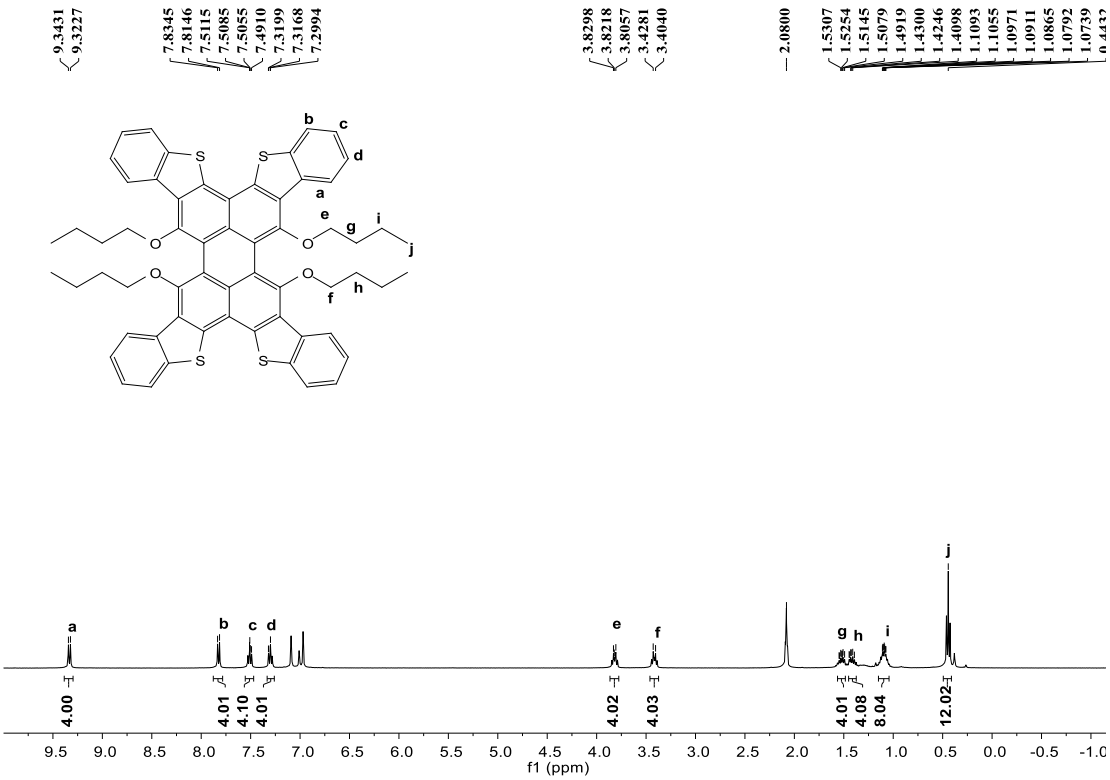

Figure S16. ^{1}H NMR spectrum (400 MHz) of compound **1** in Toluene-d_8 at 298 K.

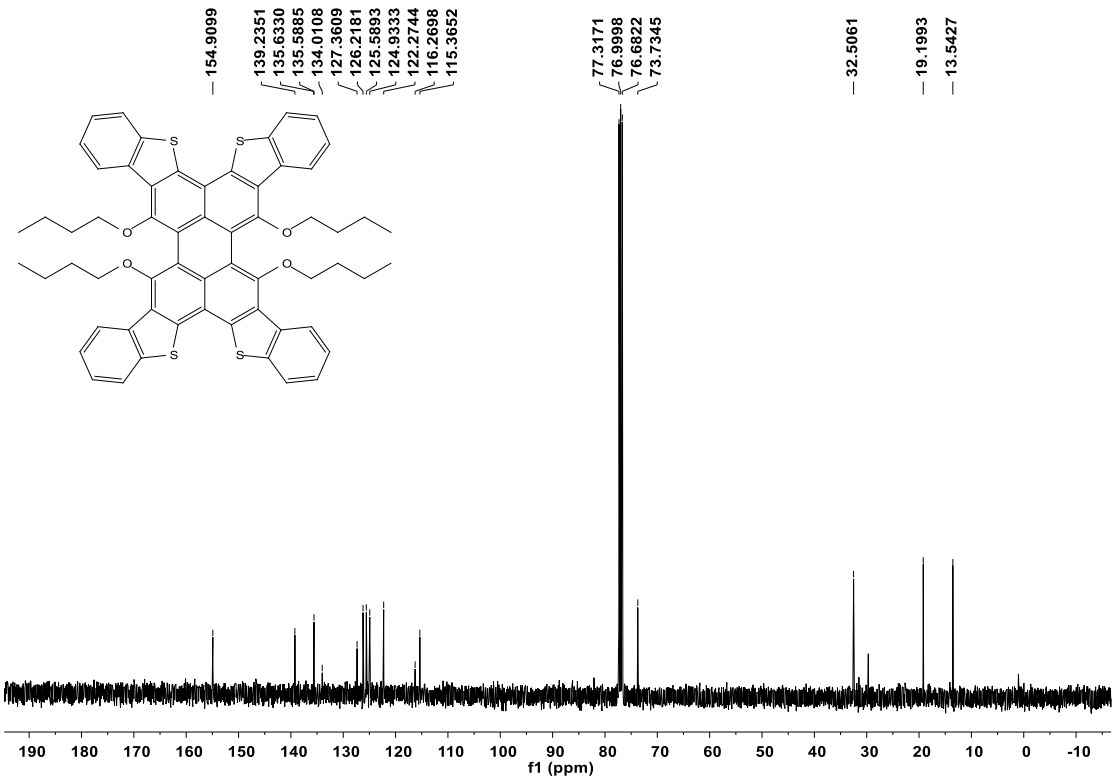

Figure S17. ^{13}C NMR spectrum (100 MHz) of compound **1** in $CDCl_3$ at 298 K.

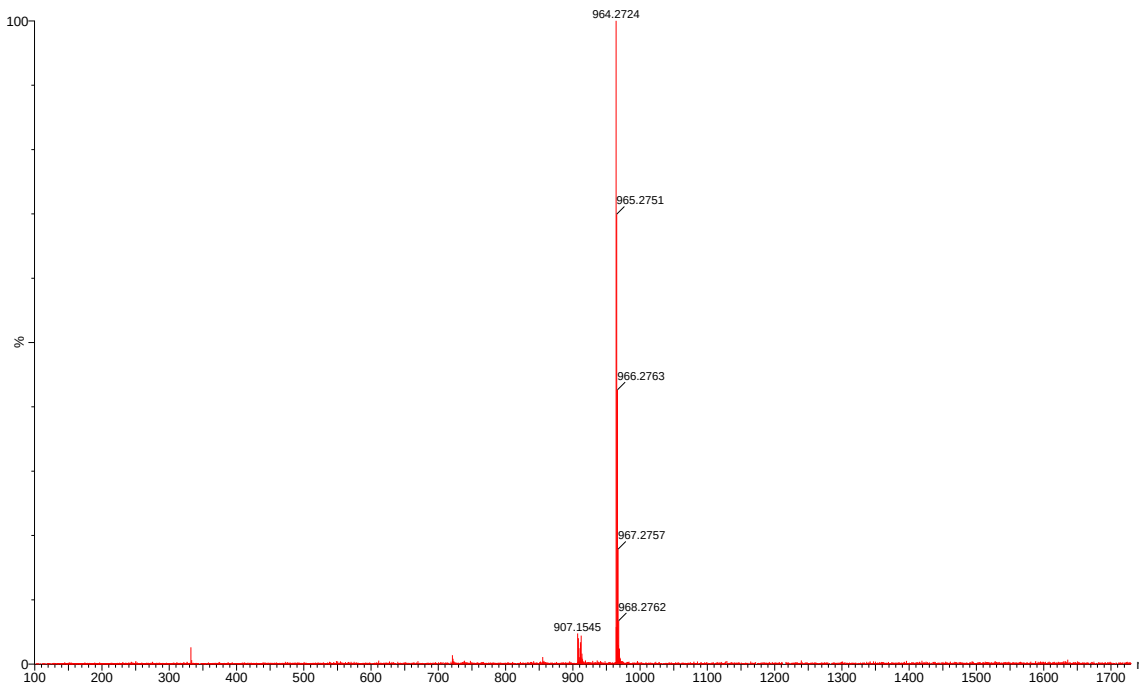

Figure S18. HR (MALDI-TOF) mass spectrum of **1**.

13. IR spectra of the products

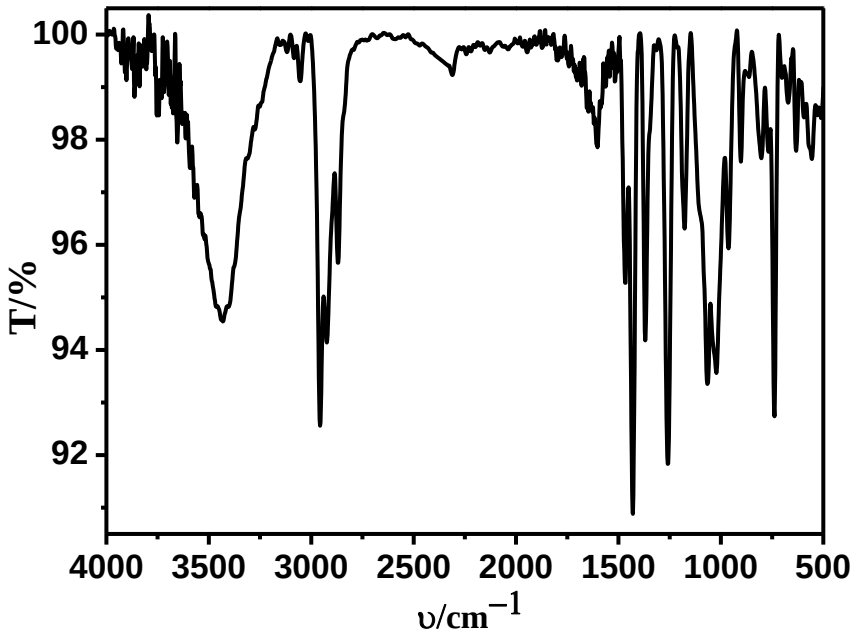

Figure S19. IR spectra of compound **2**

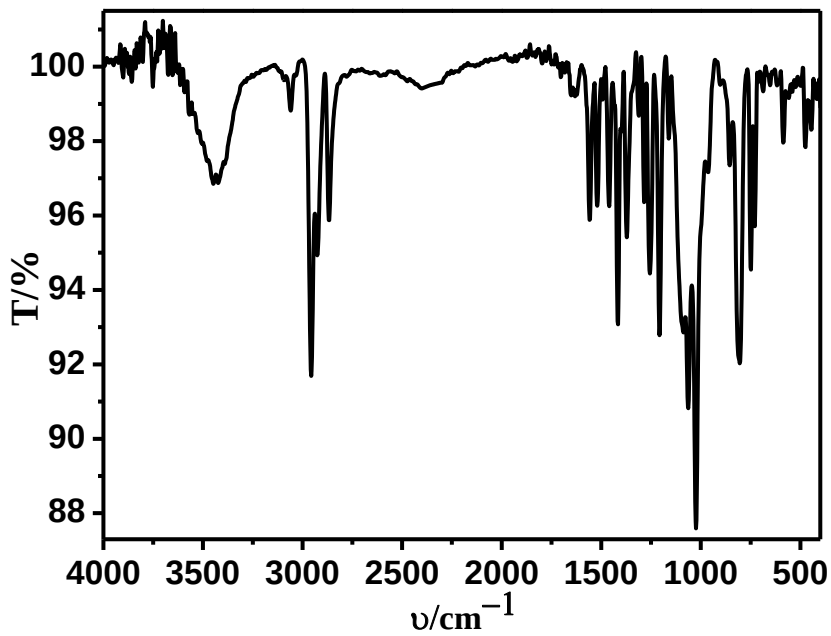

Figure S20. IR spectra of compound **1**

14. References

S1. Y. Li, Y. Hong, J. Guo, X. Huang, H. Wei, J. Zhou, T. Qiu, J. Wu, and Z. Zeng, *Org. Lett.* **2017**, *19*, 5094-5097.

S2. S. Zhang, Z. Liu, and Q. Fang, *Org. Lett*. **2017**, *19*, 1382-1385

S3. S. Zhang, X. Qiao, Y. Chen, Y. Wang, R. M. Edkins, Z. Liu, H. Li, and Q. Fang, *Org. Lett*. **2014**, *16*, 342-345.

S4. H. Sirringhaus, R. H. Friend, C. Wang, J. Leuninger, and K. Müllen, *J. Mater. Chem*. **1999,** *9*, 2095-2101.

S5. C. L. Eversloh, Z. Liu, B. Müller, M. Stangl, C. Li, and K. Müllen, *Org. Lett.* **2011**, *13*, 5528-5531.

S6. Gaussian 09, Revision D.01, M. J. Frisch, G. W. Trucks, H. B. Schlegel, G. E. Scuseria, M. A. Robb, J. R. Cheeseman, G. Scalmani, V. Barone, B. Mennucci, G. A. Petersson, H. Nakatsuji, M. Caricato, X. Li, H. P. Hratchian, A. F. Izmaylov, J. Bloino, G. Zheng, J. L. Sonnenberg, M. Hada, M. Ehara, K. Toyota, R. Fukuda, J. Hasegawa, M. Ishida, T. Nakajima, Y. Honda, O. Kitao, H. Nakai, T. Vreven, J. A. Montgomery, Jr., J. E. Peralta, F. Ogliaro, M. Bearpark, J. J. Heyd, E. Brothers, K. N. Kudin, V. N. Staroverov, T. Keith, R. Kobayashi, J. Normand, K. Raghavachari, A. Rendell, J. C. Burant, S. S. Iyengar, J. Tomasi, M. Cossi, N. Rega, J. M. Millam, M. Klene, J. E. Knox, J. B. Cross, V. Bakken, C. Adamo, J. Jaramillo, R. Gomperts, R. E. Stratmann, O. Yazyev, A. J. Austin, R. Cammi, C. Pomelli, J. W. Ochterski, R. L. Martin, K. Morokuma, V. G. Zakrzewski, G. A. Voth, P. Salvador, J. J. Dannenberg, S. Dapprich, A. D. Daniels, O. Farkas, J. B. Foresman, J. V. Ortiz, J. Cioslowski, and D. J. Fox, Gaussian, Inc., Wallingford CT, **2010**.

S7. (a) A. D. Becke, *J. Chem. Phys.* **1993**, *98*, 5648-5652; (b) C. Lee, W. Yang, and R. G. Parr, *Phys. Rev. B* **1988**, *37*, 785-789.